


Original scientific paper

SURFACE ROUGHNESS OF Ti6Al4V ALLOY PRODUCED BY LASER POWDER BED FUSIONDavid Liović¹, Marina Franulović¹, Luka Ferlič², Nenad Gubeljak²¹University of Rijeka, Faculty of Engineering, Croatia²University of Maribor, Faculty of Mechanical Engineering, Slovenia


ORCID iDs: David Liović

 <https://orcid.org/0000-0002-3608-0052>


Marina Franulović

 <https://orcid.org/0000-0002-6148-9001>

Luka Ferlič

 <https://orcid.org/0000-0002-3985-4711>

Nenad Gubeljak

 <https://orcid.org/0000-0002-3276-8431>

Abstract. Controlling the surface roughness of materials manufactured by laser powder bed fusion (L-PBF) is critical for achieving functional performance of components and improving their mechanical properties. This is important for components whose surfaces cannot be post-treated using subtractive methods. In this study, the surface roughness has been investigated by applying different laser power and scanning speed combinations. Furthermore, potential effects of different locations on the build platform have been considered as well. The regression models have been developed using significant predictor variables, with their levels defined using face-centered central composite design. The analysis of variance (ANOVA) procedure has been used to evaluate the statistical significance of factors and model performances for each prediction variable. It has been found that the average surface roughness of L-PBF Ti6Al4V alloy can be described with high fitting accuracy using laser power and scanning speed as predictor variables. The position of specimens on the build platform showed no statistically significant effect on the average surface roughness. The experimental research and statistical analysis reported in this paper will contribute to a better understanding of how position, laser power, and scanning speed influence the average surface roughness of L-PBF Ti6Al4V alloy.

Key words: Ti6Al4V alloy, L-PBF process parameters, Surface roughness, Model

1. INTRODUCTION

The possibility of achieving targeted surface roughness of components is of high interest in the scientific community and industry. It is well known that the surface roughness of materials manufactured using laser powder bed fusion (L-PBF) can be influenced by many factors involved. Therefore, the surface roughness analysis of L-PBF Ti6Al4V alloy has already been the subject of many publications [1–9]. However, the models that relate L-PBF process

Received: July 19, 2023 / Accepted September 16, 2023

Corresponding author: Marina Franulović

University of Rijeka, Faculty of Engineering, Vukovarska 58, Rijeka 51000, Croatia

E-mail: marina.franulovic@riteh.hr

parameters and surface roughness are rarely available, especially when titanium and its alloys are considered.

Surface roughness and product quality are influenced by numerous interacting factors in L-PBF process and of particular significance are: laser power, scanning speed, orientation and position of components, applied heat treatment, as well as granulation, shape and distribution of powder stock [1, 5, 10, 11]. Vaglio [2] has found that laser power and scanning speed have a stronger effect on the average surface roughness of the side surfaces, than the hatch distance. The orientation of components on the build platform highly affects surface roughness [8] and residual stresses [12], which directly reflects on the product quality. The staircase effect, which occurs due to layer-wise manufacturing is related to the surface inclination angle, highly affect the surface roughness [13–15]. The granulation, shape and distribution of the used metal powder stock have an impact on the flowability, which affects the L-PBF recoating process [8, 16, 17]. These numerous influencing factors limit the understanding of how physical processes during L-PBF affect the surface roughness.

In addition, the surface roughness of topologically simple additively manufactured components can be reduced by subsequent surface treatments. However, additive manufacturing technologies are often used in the production of topologically complex products [18–21]. Hence, subtractive post-treatments such as milling, turning and grinding, are not applicable in that case [22]. Moreover, the processing of titanium alloys is challenging [23–25]. Therefore, it is necessary to gain as much information on the influence of L-PBF process parameters on the surface roughness. To investigate and evaluate the effect of the influential factors on the surface roughness, it is necessary to have reliable and accurate measurements. However, the surface roughness measurements of metallic materials manufactured using L-PBF are challenging. More specifically, contact measurements are often performed using profilometers whose stylus scratches the surface and thus record the surface profile [26]. Considering that metals manufactured using L-PBF technologies are covered with surface-bonded particles, the movement of the stylus may be hindered due to jamming or undesired separation of loose powder particles [3]. In that case, the stylus is not able to reach the lowest and narrow surface gaps due to tip radius, and thus it is not able to completely record the surface profile, which adversely affects the measurement results. To overcome these restrictions the non-contact measurements are preferable, as they are not sensitive to contact problems. However, they can be influenced by surface reflectivity or by insufficient magnification [22, 26].

Despite significant advancements in customization of surface roughness of the L-PBF Ti6Al4V alloy have been made in recent years, the knowledge in this field remains incomplete. The studies that provide regression models for the laser power – scanning speed effect on the surface roughness and provide information on the influence of position on surface roughness are rarely available. Therefore, further research is needed to extend the existing knowledge on the possibility of influencing the surface roughness by changing the position at the build platform, or by applying different laser power and scanning speed combinations. Detailed experimental procedures are going to be carried out to investigate the surface roughness of Ti6Al4V alloy produced at different positions at the built platform by applying different laser powers and scanning speeds. For that purpose, nonlinear response surface models will be developed using the face-centered central composite design. All experimental results and nonlinear regression models will be statistically analyzed and evaluated to obtain valid results and interpretations.

2. MATERIALS AND METHODS

The manufacturing conditions have been selected according to previously reported findings described within this chapter. The specimens have been oriented vertically on the build platform during manufacturing, followed by annealing heat treatment. In this way, the warping caused by residual stresses has been minimized. Moreover, the vertical orientation eliminates the staircase effect [27], allowing investigation of the position, laser power, and scanning speed on average surface roughness. The chosen thickness of the powder layer has been set to 25 μm , to minimize the porosity as much as possible and to achieve high dimensional accuracy. The laser power and scanning speed levels have been set in the range of 200–250 W and 1000–1500 mm/s, respectively. Surface roughness measurements have been carried out using contact and non-contact methods to compare and evaluate the differences between results obtained using these two methods. In order to contribute to the accuracy of the results and their repeatability, applied design of experiments, utilized powder stock, L-PBF process and its parameters, specimen dimensions and surface roughness measurements are detailed.

2.1. Design of experiments and model development

Face-centered central composite design (FC-CCD) of experiments has been used to define the laser power and scanning speed levels utilized in the L-PBF process. This design has star points at the center of each face of the factorial space [28]. Hence, it requires three levels for each predictor variable as shown in Table 1. Central composite design has proven to be effective for modeling the influence of process parameters of many manufacturing technologies [29–32]. In addition, specimens have been divided into four groups representing their positions on the build platform (Pos 1, Pos 2, Pos 3 and Pos 4). This experimental design provides a reasonable balance between the number of experiments required and the information obtained.

Table 1 Parameters and their levels used in design of experiments

Parameters	Symbol	Levels		
		-1	0	1
Laser power (W)	P	200	225	250
Scanning speed (mm/s)	v	1000	1250	1500

For each prediction variable, response surface model coefficients have been found using Ordinary Least Square (OLS) method. The 95% confidence intervals have been determined for each prediction variable using the following equation [33]:

$$\mu_{y|x_0} = \hat{y}(x_0) \pm t_{\alpha/2, df(error)} \sqrt{\hat{\sigma}^2 \cdot \mathbf{x}'_0 (\mathbf{X}'\mathbf{X})^{-1} \mathbf{x}_0}. \quad (1)$$

where $\hat{y}(x_0)$ is the estimated mean response at the grid point, \mathbf{x}_0 is a vector containing grid points, \mathbf{X} is a model matrix consisting of the levels of the independent variables expanded to model form, $\hat{\sigma}^2$ is the estimate of the error variance, and $t_{\alpha/2, df(error)}$ is the t -value related to the desired level of confidence and the residuals' degrees of freedom.

Since regression models are used for approximations of complex physical phenomena, there is a high possibility that more than one model will fit data with a suitable accuracy [34]. In general, models with higher complexity have better fitting performances. However,

they also have a higher degree of interdependence between model parameters, when compared to more simple models [34]. Therefore, it is justified to increase the number of parameters only in the case when the more complex model provides significantly better fit than the simpler model. In that context, two models will be given for each prediction variable, tested using multiple statistical tests, compared, and their fitting performance and complexity will be described in detail. The first model given for each variable has better fitting performance, but it also has a higher complexity. On the other hand, the second model has a lower complexity, which is desirable, but it has a lower fitting performance as well. Using this approach, the influence of model parameters will be investigated, and significant model parameters will be identified for each prediction variable. This will result in four regression models (M1 – M4), which will be compared, evaluated, and discussed in detail. It is worth noting that the second proposed models (i.e., models with lower complexity), will be designed by eliminating the non-significant terms.

2.2. Test specimens

The tensile test specimens have been used for surface roughness measurements. A total of 36 test specimens (Fig. 1a) have been used, ensuring 4 repetitions for each utilized L-PBF process parameter combination. Specimen groups and their respective positions on the build platform are shown in Figure 1b. The dimensions of tensile test specimens have been modified based on rectangular test specimen geometry stated in ASTM E8 / E8M - 16a [35], by maintaining the recommended ratio of gauge length and width of 5:1. Therefore, the gauge length and width have been 20 mm and 4 mm respectively, while the length of the reduced parallel section has been 22 mm, as can be seen in Fig. 1a. The surface roughness measurements have been performed on the reduced parallel section ($22 \times 4 \text{ mm}^2$) marked with a blue square.

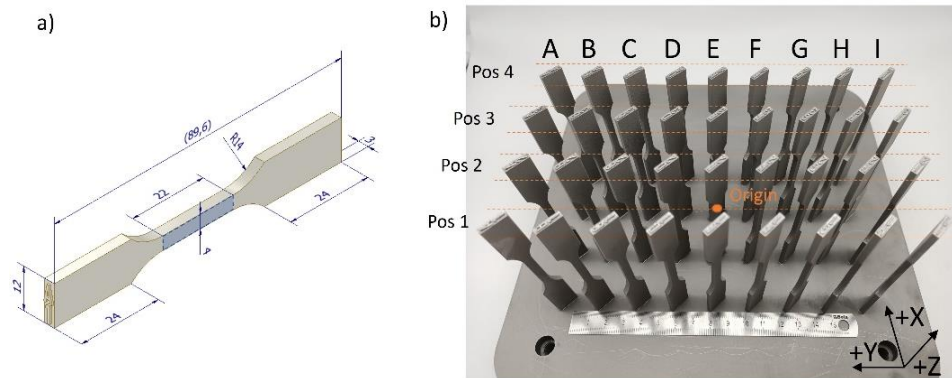


Fig. 1 a) Test specimen dimensions and highlighted region where surface roughness measurements have been performed, b) Position, orientation and corresponding IDs of test specimens

2.3. Laser powder bed fusion and heat treatment

The test specimens have been positioned vertically on the build platform, as can be seen in Fig. 1b. The coordinates of each specimen placed on the build platform are given in

Table 2. All reported coordinates represent the position of specimen respect to the origin (mid-point) of the build platform. The specimens have been rotated around Z-axis by 45° to ensure that the recoater does not encounter a straight wall while moving across all specimens, as can be seen in Fig. 1b.

Table 2 Coordinates of each specimen respect to the origin (mid-point) of the build platform

	Position 1									Position 2								
	A1	B1	C1	D1	E1	F1	G1	H1	I1	A2	B2	C2	D2	E2	F2	G2	H2	I2
X	-70	-70	-70	-70	-70	-70	-70	-70	-70	-40	-40	-40	-40	-40	-40	-40	-40	-40
Y	88	66	44	22	0	-22	-44	-66	-88	88	66	44	22	0	-22	-44	-66	-88
	Position 3									Position 4								
	A3	B3	C3	D3	E3	F3	G3	H3	I3	A4	B4	C4	D4	E4	F4	G4	H4	I4
X	-10	-10	-10	-10	-10	-10	-10	-10	-10	20	20	20	20	20	20	20	20	20
Y	88	66	44	22	0	-22	-44	-66	-88	88	66	44	22	0	-22	-44	-66	-88

In this research the extra low interstitial Ti6Al4V (ELI) Grade 23 powder with spherical particles has been used (Fig. 2a). To determine the particle size distribution of the powder, 530 measurements have been performed using Keyence VHX 7000 microscope. Diameters of powder sample particles have been in range from ~4 µm to ~48 µm (Fig. 2b) with a median diameter of 27.06 µm. The 10th and 90th percentiles were 12.98 µm and 38.92 µm, respectively.

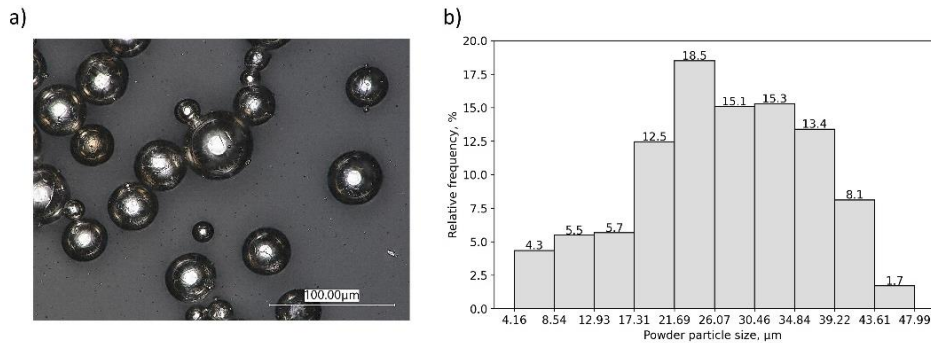


Fig. 2 Utilized Ti6Al4V (ELI) Grade 23 powder: a) Powder particles, b) Size distribution of powder particles

Test specimens have been manufactured using Concept Laser M2 Cusing machine equipped with a 400 W single-mode CW ytterbium-doped fibre laser. The L-PBF process has been performed under argon atmosphere to keep oxygen level below 0.2%. The L-PBF process parameters used in this study for manufacturing of test specimens are listed in Table 3. Each group of specimens is denoted using an ID in the form of a capital letter in the range A – I, which represents a specific combination of utilised L-PBF process parameters. Laser power and scanning speed levels have been defined using face-centred central composite design to investigate their effect on surface roughness.

Table 3 L-PBF process parameters utilized for L-PBF of Ti6Al4V alloy

Variation levels									
Laser power (P), W	200			225			250		
Scanning speed (v), mm/s	1000	1250	1500	1000	1250	1500	1000	1250	1500
Energy density (E_d), J/mm ³	88.9	71.1	59.3	100	80	66.7	111.1	88.9	74.1
Linear energy density (E_L), J/mm	0.2	0.16	0.13	0.23	0.18	0.15	0.25	0.2	0.17
Specimen group (ID)	A	B	C	D	E	F	G	H	I
Number of test specimens	4	4	4	4	4	4	4	4	4
Constant L-PBF process parameters									
Layer thickness (t)	0.025 mm								
Hatch distance (h)	0.09 mm								
Laser spot diameter (d)	0.1 mm								
Scanning strategy	Bi-directional, single pass, 90° rotation of scan vector between layers								

Laser power (P) and scanning speed (v) levels have been selected according to previous research findings on appropriate range of linear energy density ($E_L = P/v$) that ensures successful L-PBF of Ti6Al4V alloy [36]. As stated in [36], linear energy densities in 0.1 – 0.2 J/mm range provide the best candidates for successful production of bulk parts. Therefore, the laser power and scanning speed levels have been carefully defined to ensure that the center point of the utilized FC-CCD remained within the specified range. The remaining points have been set either inside or close to the recommended interval. These process parameters ensure a stable L-PBF process, thus enabling development of reliable regression models. It is important to note that a wider range of parameters could result in completely different melting modes [36, 37], which would influence surface roughness values differently [9]. In such cases, employing a single regression model may not be appropriate, as different melting modes would have different effects on surface roughness. Therefore, the laser power and scanning speed levels have been carefully selected to ensure consistent melting modes for each combination and to enable the manufacturability of bulk parts.

The annealing heat treatment under argon atmosphere has been applied with a heating rate of 3.5 °C/min until the temperature reaches 840 °C. The specimens have been held at the temperature of 840 °C for 120 minutes. Specimens have been cooled in the furnace under argon atmosphere down to 150 °C with corresponding cooling time from 800°C to 500 °C ($\Delta t_{8/5}$) equal to 290 min. The annealing heat treatment has been selected, since it is the most preferred heat treatment used for L-PBF Ti6Al4V alloy due to its effectiveness in residual stress relaxation and ductility increase [38–40]. The heat treatment parameters have been chosen based on the guidelines provided by the manufacturers of the L-PBF machine.

2.4. Surface roughness measurements

Surface roughness generally refers to the deviations in surface height relative to a reference plane [41]. The average surface roughness (R_a) measurements have been performed on test specimens using TESA Rugosurf 10-G profilometer. Prior to surface roughness measurements, all specimens have been cleaned in an ultrasonic bath for 10 minutes in distilled water to remove loose particles from the surface that may adversely affect the measurement reliability. Measurements have been repeated 6 times along the gauge length of specimen's surface (Fig. 3a) to make results reliable. The profile filter has

been selected according to ISO 4288:1996 and ISO 3274:1996 standards [42, 43]. Therefore, traverse length (l_t) has been set to 15 mm, evaluation length (l_n) to 12.5 mm, cut-off (λ_c) and sampling length (l_r) to 2.5 mm, and short-wave profile filter (λ_s) to 8 μm .

The area average surface roughness (S_a) measurement parameters have been obtained using Keyence VHX 7000 microscope. The S-filter value has been set to 25 μm ($\sim 3 \times$ pixel size) when magnification of 1000 \times has been used. The L-filter value has been set to 2.5 mm according to the findings stated in [26, 44]. Prior to the area average surface roughness (S_a) measurements, sensitivity analysis has been performed by scanning the same area using different vertical pitch and magnification levels, as shown in Fig. 3b. Note that the error bars are omitted in Fig. 3b, since the results represent the identical area, but scanned using different magnification and vertical pitch values.

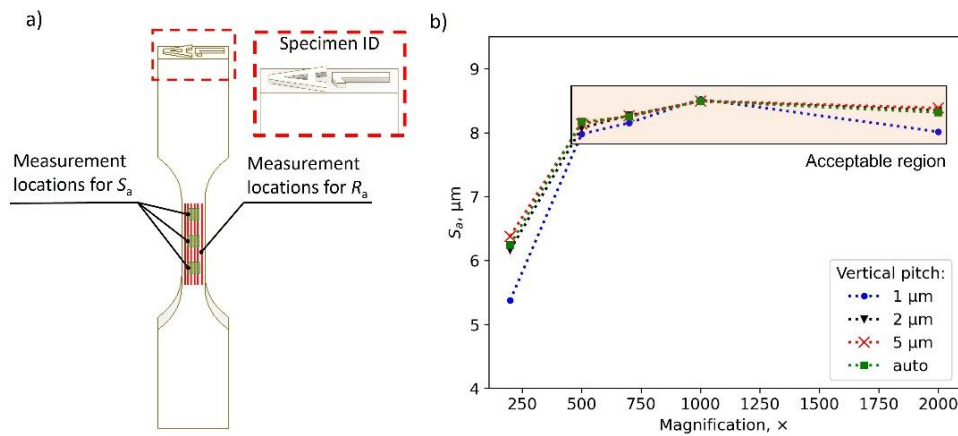


Fig. 3 a) Measurement locations and specimen orientation for S_a and R_a , b) The influence of the magnification and vertical pitch values on S_a

In general, higher magnifications generate more robust and reliable results since the quality of the details of the scanned surface is higher. However, in that case the microscope scanning time and data processing are extremely time consuming. Therefore, a certain compromise between the appropriate measurement accuracy and time resources should be found. From the results shown in Fig. 3b it is evident that the magnifications equal or higher than 500 \times give similar S_a values which is in accordance with findings stated in [22]. The vertical pitch had the smallest influence on the results when a magnification of 1000 \times has been used. Therefore, based on results from the sensitivity analysis, magnification of 1000 \times and vertical pitch of 1 μm have been selected for further measurements. The area surface roughness measurements, used in response surface analysis, have been performed three times on each specimen's gauge length, by scanning and evaluating the area of $2 \times 2 \text{ mm}^2$ at three different locations as shown on Fig. 3a.

3. RESULTS AND DISCUSSION

All reported values within this study are expressed in the form of mean value (standard deviation). Furthermore, on all response surface figures, models with higher R^2 values have been shown to enable a visual assessment of utilized laser power and scanning speed levels on the prediction variables. In that way, a visual assessment for both predictor variables will be enabled. The surface roughness measurements have been performed on one specimen (H2 specimen) before and after ultrasonic cleaning to consider its potential influence on results. Before ultrasonic cleaning the average surface roughness has been $6.670 \mu\text{m}$ (std. $0.406 \mu\text{m}$), and after ultrasonic cleaning $6.788 \mu\text{m}$ (std. $0.389 \mu\text{m}$). The ultrasonic cleaning showed no effect on the average surface roughness measurements, given that means and standard deviations have been almost identical.

The dependence of R_a and S_a values on specimen positions has been evaluated using the Kruskal-Wallis rank sum test as R_a and S_a were not normally distributed in all specimen groups. The equality of variances between specimen groups has been tested using Levene's test, both on R_a and S_a data. The variances have been equal, as the calculated p -values for R_a and S_a data were 0.84 and 0.79 respectively. The calculated p -values using Kruskal-Wallis test for R_a and S_a values have been 0.80 and 0.90, respectively. It indicates that the different positions do not have statistically significant effect on R_a and S_a values, which can be seen in Fig. 4 as well. This result is in accordance with findings stated in [2], where it was demonstrated that the laser power and scanning speeds are the most relevant factors influencing the side surface roughness. Therefore, further regression models for surface roughness can be developed using only P and v as predictor variables.

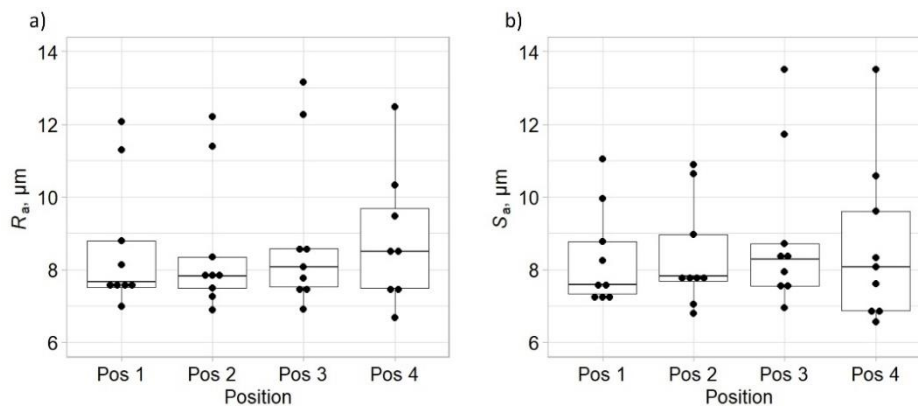


Fig. 4 Influence of different positions on the variation of: a) R_a values, b) S_a values

By testing models M1 and M2 against each other using ANOVA procedure with respect to their fitting ability (i.e., testing whether the difference between residual sum of squares of each model is statistically significant) it has been found that model M1 does not provide a better fit than model M2, since the calculated p -value using ANOVA procedure was 0.581 which is higher than a level of significance ($\alpha = 0.05$). Therefore, the influence of P and v on average surface roughness (R_a) can be described efficiently without term v^2 . This can be seen in Table 4, where p -values have been reported for each parameter used to develop model M1.

Table 4 Parameters of M1 full quadratic model with corresponding p -values

M1		
Source	p -value	Remark
Intercept	< 0.001	significant
P	< 0.001	significant
v	< 0.001	significant
P^2	< 0.001	significant
v^2	0.58	not significant
Pv	< 0.001	significant

Both models developed for R_a have homoscedastic variance in the error term (p -value > 0.05 in both cases) which has been confirmed using non-constant variance (NCV) score test, as shown in Table 5. It indicates that utilized levels of predictors do not affect the variance of model errors, further validating the applicability of the OLS regression method. This test also confirms that R_a can be efficiently modelled using both models across the whole P and v range specified within design of experiments (DoE), since equal model error variance has been present. Furthermore, both models have normally distributed studentized residuals as p -values determined using Shapiro-Wilk (S-W) normality test have been in both cases larger than 0.05, which is a prerequisite for a valid application of the OLS regression method. As can be seen in Table 5, both models have high R^2 and adjusted R^2 values. The influence of P and v on R_a has been shown on Fig. 5a with a superimposed 95% confidence intervals calculated using Eq. (1).

Table 5 Regression models for R_a and their statistical properties

Average surface roughness (R_a)		R^2	Adj. R^2	p -value (NCV)	p -value (S-W)
M1	$R_a = 0.0021P^2 - 2.721 \times 10^{-6}v^2 - 0.7686P + 0.0563v - 0.0002Pv + 65.154$	0.852	0.827	0.417	0.074
M2	$R_a = 0.0021P^2 - 0.7686P + 0.0495v - 0.002Pv + 69.2928$	0.850	0.831	0.297	0.057

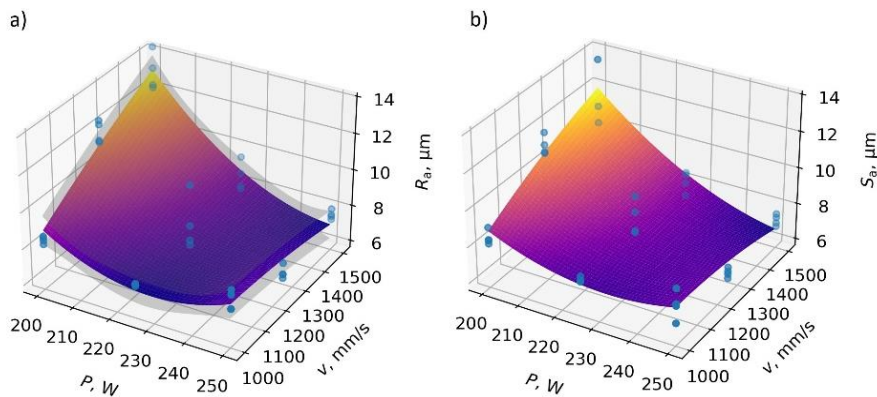


Fig. 5 Response surfaces describing the influence of P and v on the: a) Line average surface roughness (R_a) values with superimposed 95% confidence intervals visible as gray surfaces, b) Area average surface roughness (S_a) values with added experimental data visible as blue dots

Testing of the area average surface roughness (S_a) models against each other using the ANOVA procedure revealed that model M3 does not have a better fit than model M4 (p -value = 0.406). Therefore, the influence of P and v on S_a can be described efficiently without term v^2 . The p -values for each parameter used to develop model M3 are reported in Table 6. However, in this case both models have heteroscedastic variance of error term since p -values are lower than 0.05, as can be seen in Table 6.

Hence, heteroskedasticity-robust procedure (HC3 method) is applied to evaluate model coefficients obtained using OLS method. The analysis confirmed the validity of the previously determined model coefficients stated in Table 6. Consequently, confidence intervals have been omitted from Fig. 5b since the assumption of equal variance of residuals has been violated. Therefore, on Fig. 5b only the scatter plot has been added to the response surface plot to visualize both experimentally measured data and corresponding nonlinear regression model M3.

Table 6 Parameters of M3 full quadratic model with corresponding p -values

M3		
Source	p -value	Remark
Intercept	< 0.001	significant
P	< 0.001	significant
v	0.004	significant
P^2	0.007	significant
v^2	0.41	not significant
Pv	< 0.001	significant

Table 7 Regression models for S_a and their statistical properties

Area average surface roughness (S_a)		R^2	Adj. R^2	p -value (NCV)	p -value (S-W)
M3	$S_a = 0.0014P^2 - 4.123 \times 10^{-6}v^2 - 0.4884P + 0.0505v - 0.0002Pv + 37.256$	0.802	0.769	< 0.001	-
M4	$S_a = 0.0014P^2 - 0.4884P + 0.0402v - 0.0002Pv + 43.526$	0.797	0.771	< 0.001	-

As expected, a strong linear relation between experimentally measured R_a values using contact profilometer and S_a values measured using microscope is present ($r = 0.948$). Relation between R_a and S_a values can be visualized by comparing the shapes of the response surfaces, on Fig. 5a and b. It is evident that the shape and the curvature of the response surfaces are almost identical, which confirms the relation between those two observed predictions. Both R_a and S_a reach their maximum values for the C group of specimens, i.e., when $P = 200$ W and $v = 1500$ mm/s have been used for the L-PBF of Ti6Al4V alloy. In that case, R_a and S_a values have been $12.937 \mu\text{m}$ (std. $1.039 \mu\text{m}$) and $11.966 \mu\text{m}$ (std. $1.821 \mu\text{m}$), respectively.

This occurrence is attributed to the stacking and incomplete melting of powder particles near the specimen's surfaces due to the lowest utilized energy input (59.3 J/mm^3), which is in accordance with findings stated in [2]. When surface topographies of the C group of specimens (i.e., specimen group with the highest mean R_a and S_a values) and I group of specimens (i.e., specimen group with the lowest mean R_a and S_a values) are compared in Fig. 6a and b, it is evident that the C group of specimens has higher peaks with a maximum value up to $119.4 \mu\text{m}$.

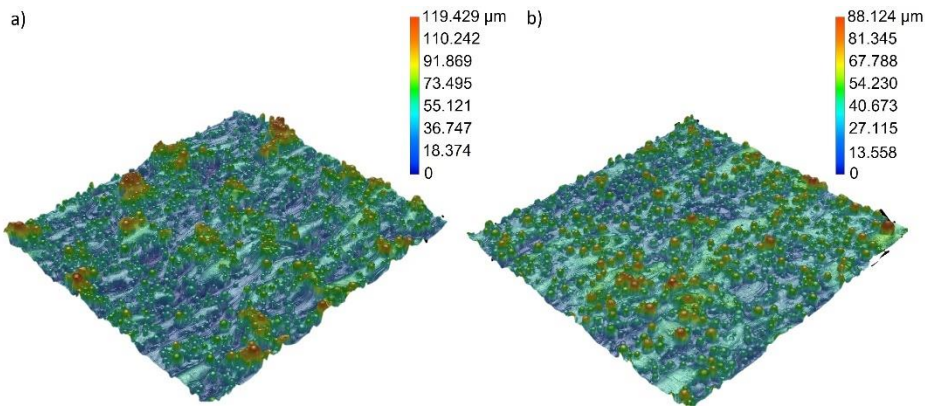


Fig. 6 a) Group of specimens C characteristic by the highest measured R_a and S_a values, b) Group of specimens I characteristic by the lowest measured R_a and S_a values

High values of coefficients of variation (COV), specific to C group of specimens (8.03% for R_a and 15.22% for S_a), also imply that more incomplete and unequal melting of powder particles is present in contrast to I group of specimens that has lower COV values (3.26% for R_a and 4.36% for S_a). More specifically, I group has R_a and S_a values of 7.612 μm (std. 0.248 μm) and 7.195 μm (std. 0.314 μm), respectively. This leads to the conclusion that the surface roughness of specimens in group C is lower and more uniform than surface roughness of specimens in the I group.

Except for the used L-PBF process parameters, surface roughness of products manufactured using the L-PBF technology predominantly depends on the powder particle size distribution [45], inclination angle with respect to the build platform [5], and heat treatment [11]. Thus, in the literature, wide ranges of resulting average surface roughness values of L-PBF Ti6Al4V specimens have been reported by different groups of authors [1, 9, 46, 47]. When process parameters are considered, Mierzejewska et al. [11] found that energy densities in the range from 88 to 113 J/mm^3 lead to surface roughness decrease, while energy densities in the range from 44 to 63 J/mm^3 causes surface roughness increase. This is valid in the case when only one predictor variable is considered within DoE, as demonstrated in [11]. However, similar or identical values of energy densities can be obtained using completely different combinations of P and v , as can be seen in Table 3. Hence, energy density cannot be isolated and independently used for interpretation of results when two predictor variables (i.e., P and v) are involved [48]. Therefore, results have been interpreted by separately observing the effect of P and v on considered prediction variables, as shown in Fig. 6a and b. When the influence of scanning speed on the R_a and S_a values is considered, its effect is more pronounced when the lowest utilized laser power level has been used (i.e., 200 W). More specifically, the increase in laser power levels reduces the effect of the scanning speed on the R_a and S_a values. It is also evident that the decrease in scanning speed levels reduces laser power's influence on the R_a and S_a values. Therefore, when low surface roughness of the Ti6Al4V L-PBF parts is desired, the higher laser power values should be considered. This finding is consistent with the previously published studies, where the decrease in R_a and S_a with an increase in laser power has been found [2, 49]. Elsayed et al. [50] have reported the same effect at substantially lower laser powers ranging from 35 to 50 W, where significant drop of R_a with laser power increase has

been found. As reported in [51, 52], increasing the laser power leads to an increase in energy density, which enhances the wettability of the melt pool. This occurrence reduces the differences in surface tensions and subsequently decreases the balling effect [50, 51]. As a result, there is a decrease in the formation of irregular beads or spherical drops, leading to a reduction in average surface roughness. In order to decrease the average surface roughness of the top and side surfaces, the higher laser powers should be used [52, 53]. As stated by Mumtaz et al. [52], the higher laser powers promote the flattening of the melt pool surface and enhance its wettability which reduces the chances of the balling effect to occur.

4. CONCLUSIONS

The average surface roughness of the L-PBF Ti6Al4V alloy has been systematically studied through experimental tests, followed by comprehensive regression analysis and model verification. Consequently, nonlinear regression models have been developed to relate laser power and scanning speed with average surface roughness. Moreover, the influence of position, laser power, and scanning speed on average surface roughness has been interpreted. The findings of this study are relevant to the L-PBF manufacturing of Ti6Al4V alloy, specifically when employing laser powers ranging from 200 to 250 W and scanning speeds ranging from 1000 to 1500 mm/s.

The influence of laser power and scanning speed on the average surface roughness of the L-PBF Ti6Al4V alloy can be interpreted and described with high precision using nonlinear regression models that include two predictor variables (i.e., laser power and scanning speed). More specifically, laser power and scanning speed significantly influence the average surface roughness values. By using higher laser powers, it is possible to reduce average surface roughness and decrease the effect of scanning speed. The influence of specimen position on the build platform showed to be non-significant for the average surface roughness. The results gained as part of this systematically conducted experimental research, supported by comprehensive statistical analysis, will contribute to a better understanding of the influence of L-PBF process parameters on the surface roughness of the widely used Ti6Al4V alloy.

Acknowledgement: *This work has been supported by Croatian Science Foundation under the project number IP-2019-04-3607 and by University of Rijeka under project number uniri-tehnic-18-34. Part of the work presented in this research has been supported by using the equipment acquired through the Research program P2-0137 "Numerical and experimental analysis of mechanical systems" funded by Slovenian Research Agency-ARRS. The authors would like to thank LAMA FVG and Dr. Ing. Emanuele Vaglio PhD for L-PBF of test specimens and technical assistance.*

REFERENCES

1. Pal, S., Gubelj, N., Hudak, R., Lojen, G., Rajtukova, V., Predan, J., Kokol, V., Drstvenšek, I., 2019, *Tensile properties of selective laser melting products affected by building orientation and energy density*, Materials Science and Engineering A, 743, pp. 637-647.
2. Vaglio, E., 2018, *Research on Process Parameter Optimization in Selective Laser Melting*, PhD Thesis, University of Udine, 202 p.
3. Molinari, A., Ancellotti, S., Fontanari, V., Iacob, E., Luchin, V., Zappini, G., Benedetti, M., 2022, *Effect of process parameters on the surface microgeometry of a Ti6Al4V alloy manufactured by laser powder bed fusion: 3D vs. 2D characterization*, Metals, 12(1), 106.

4. Dareh Baghi, A., Nafisi, S., Hashemi, R., Ebendorff-Heidepriem, H., Ghomashchi, R., 2023, *A New Approach to Empirical Optimization of Laser Powder Bed Fusion Process for Ti6Al4V Parts*, Journal of Materials Engineering and Performance.
5. Chen, Z., Wu, X., Tomus, D., Davies, C.H.J., 2018, *Surface roughness of Selective Laser Melted Ti-6Al-4V alloy components*, Additive Manufacturing, 21, pp. 91-103.
6. Pasang, T., Tavlovich, B., Yannay, O., Jackson, B., Fry, M., Tao, Y., Turangi, C., Wang, J., Jiang, C., Sato, Y., Tsukamoto, M., Misiolek, W.Z., 2021, *Directionally-Dependent Mechanical Properties of Ti6Al4V Manufactured by Electron Beam Melting (EBM) and Selective Laser Melting (SLM)*, Materials, 14(13), 3603.
7. Wang, D., Dou, W., Yang, Y., 2018, *Research on selective laser melting of Ti6Al4V: Surface morphologies, optimized processing zone, and ductility improvement mechanism*, Metals, 8(7), 471.
8. Chen, Z., Wu, X., Davies, C.H.J., 2021, *Process variation in Laser Powder Bed Fusion of Ti-6Al-4V*, Additive Manufacturing, 41, 101987.
9. Buhairi, M.A., Foudzi, F.M., Jamhari, F.I., Sulong A.B., Radzuan, N.A.M., Muhamad, N., Mohamed, I.F., Azman, A.H., Harun, W.S.W., Al-Furjan, M.S.H., 2023, *Review on volumetric energy density: influence on morphology and mechanical properties of Ti6Al4V manufactured via laser powder bed fusion*, Progress in Additive Manufacturing, 8(2), pp. 265-283.
10. Gu, D.D., Meiners, W., Wissenbach, K., Poprawe, R., 2012, *Laser additive manufacturing of metallic components: Materials, processes and mechanisms*, International Materials Reviews, 57(3), pp. 133-164.
11. Mierzejewska, Z.A., Hudák, R., Sidun, J., 2019, *Mechanical properties and microstructure of DMLS Ti6Al4V alloy dedicated to biomedical applications*, Materials, 12(1), 176.
12. Sander, G., Babu, A.P., Gao, X., Jiang, D., Birbilis, N., 2021, *On the effect of build orientation and residual stress on the corrosion of 316L stainless steel prepared by selective laser melting*, Corrosion Science, 179, 109149.
13. Kim, W.Y., Yoon, E.Y., Kim, J.H., Kim, S., 2023, *Surface Characteristics of Ti-6Al-4V Alloy Based on the Process Parameter and Abrasive Process in the Laser Powder Bed Fusion*, Metals and Materials International, 29(8), pp. 2345-2357.
14. Foti, P., Mohammad Javad Razavi, S., Fatemi, A., Berto, F., 2023, *Multiaxial fatigue of additively manufactured metallic components: A review of the failure mechanisms and fatigue life prediction methodologies*, Progress in Materials Science, 137, 101126.
15. Kokare, S., Oliveira, J.P., Godina, R., 2023, *Life cycle assessment of additive manufacturing processes: A review*, Journal of Manufacturing Systems, 68, pp. 536-559.
16. Gokuldoss, P.K., Kolla, S., Eckert, J., 2017, *Additive manufacturing processes: Selective laser melting, electron beam melting and binder jetting-selection guidelines*, Materials, 10(6), 672.
17. Chekotu, J.C., Groarke, R., O'Toole, K., Brabazon, D., 2019, *Advances in selective laser melting of Nitinol shape memory alloy part production*, Materials, 12(5), 809.
18. Alaimo, A., Marino, F., Valvano, S., 2021, *BCC lattice cell structural characterization*, Reports in Mechanical Engineering, 2(1), pp. 77-85.
19. Mendricky, R., Soni, R.D., 2022, *Geometric Stability of Parts Produced by 3D Printing*, Tehnički Vjesnik, 29(1), pp. 23-29.
20. Lvov, V.A., Senatov, F.S., Shinkaryov, A.S., Chernyshikhin, S.V., Gromov, A.A., Sheremetyev, V.A., 2023, *Experimental 3D printed re-entrant auxetic and honeycomb spinal cages based on Ti-6Al-4V: Computer-Aided design concept and mechanical characterization*, Composite Structures, 310, 116766.
21. Stojković, J.R., Stojković, M., Turudija, R., Arandelović, J., Marinkovic, D., 2023, *Adjustable Elasticity of Anatomically Shaped Lattice Bone Scaffold Built by Electron Beam Melting Ti6Al4V Powder*, Metals, 13(9), 1522.
22. Lee, S., Rasoolian, B., Silva, D.F., Pegues, J.W., Shamsaei, N., 2021, *Surface roughness parameter and modeling for fatigue behavior of additive manufactured parts: A non-destructive data-driven approach*, Additive Manufacturing, 46, 102094.
23. Akıncioğlu, S., 2022, *Taguchi Optimization of Multiple Performance Characteristics in the Electrical Discharge Machining of the TiGr2*, Facta Universitatis Series Mechanical Engineering, 20(2), pp. 237-253.
24. Sidhu, A.S., 2021, *Surface texturing of non-toxic, biocompatible titanium alloys via electro-discharge*, Reports in Mechanical Engineering, 2(1), pp. 51-56.
25. Zhang, C., Zou, D., Mazur, M., Mo, J.P.T., Li, G., Ding, S., 2023, *The State of the Art in Machining Additively Manufactured Titanium Alloy Ti-6Al-4V*, Materials, 16(7), 2583.
26. Triantaphyllou, A., Giusca, C.L., Macaulay, G.D., Roerig, F., Hoebel, M., Leach, R.K., Tomita, B., Milne, K.A., 2015, *Surface texture measurement for additive manufacturing*, Surface Topography: Metrology and Properties, 3(2), 024002.
27. Yan, X., Gao, S., Chang, C., Huang, J., Khanlari, K., Dong, D., Ma, W., Fenineche, N., Liao, H., Liu, M., 2021, *Effect of building directions on the surface roughness, microstructure, and tribological properties of selective laser melted Inconel 625*, Journal of Materials Processing Technology, 288, 116878.
28. Heckert, N., Filliben, J., Croarkin, C., Hembree, B., Guthrie, W., Tobias, P., Prinz, J., 2002, *Handbook 151: NIST/SEMATECH e-Handbook of Statistical Methods*, NIST Interagency/Internal Report (NISTIR), Gaithersburg, Maryland.

29. Kumar, R., Upadhyay, V., Sharma, C., 2022, *Modeling and Optimization of Process Parameters for Friction Stir Welding of Dissimilar Aerospace Alloys AA2014 and AA7075*, Engineering Review, 42(2), pp. 59-78.
30. Vasantha Kumar, K.P., Balasubramanian, M., 2022, *Multi-Response Optimization of FSW Parameters for Dissimilar Al-Mg Alloys*, Tehnički Vjesnik, 29(3), pp. 926-932.
31. Gunjal, S.B., Pawar, P.J., 2020, *Improving the process performance of magnetic abrasive finishing of SS304 material using multi objective artificial bee colony algorithm*, Engineering Review, 41(1), pp. 34-49.
32. Mulhi, A., Dehgahi, S., Waghmare, P., Qureshi, A.J., 2023, *Process Parameter Optimization of 2507 Super Duplex Stainless Steel Additively Manufactured by the Laser Powder Bed Fusion Technique*, Metals, 13(4), 725.
33. Myers, R.H., Montgomery, D.C., Anderson-Cook, C.M., 2016, *Response Surface Methodology: Process and Product Optimization Using Designed Experiments*, Wiley, Hoboken, 856 p.
34. Jaqaman, K., Danuser, G., 2006, *Linking data to models: Data regression*, Nature Reviews Molecular Cell Biology, 7(11), pp. 813-819.
35. ASTM E8/E8M -16a, 2016, *Standard Test Methods for Tension Testing of Metallic Materials*.
36. Vaglio, E., De Monte, T., Lanzutti, A., Totis, G., Sortino, M., Fedrizzi, L., 2020, *Single tracks data obtained by selective laser melting of Ti6Al4V with a small laser spot diameter*, Data in Brief, 33, 106443.
37. Bergmueller, S., Gerhold, L., Fuchs, L., Kaserer, L., Leichtfried, G., 2023, *Systematic approach to process parameter optimization for laser powder bed fusion of low-alloy steel based on melting modes*, International Journal of Advanced Manufacturing Technology, 126, pp. 4385-4398.
38. Singla, A.K., Banerjee, M., Sharma, A., Singh, J., Bansal, A., Gupta, M.K., Khanna, N., Shahi, A.S., Goyal, D.K., 2021, *Selective laser melting of Ti6Al4V alloy: Process parameters, defects and post-treatments*, Journal of Manufacturing Processes, 64, pp. 161-187.
39. Jamhari, F.I., Foudzi, F.M., Buhairi, M.A., Sulong, A.B., Mohd Radzuan, N.A., Muhamad, N., Mohamed, I.F., Jamadon, N.H., Tan, K.S., 2023, *Influence of heat treatment parameters on microstructure and mechanical performance of titanium alloy in LPBF: A brief review*, Journal of Materials Research and Technology, 24, pp. 4091-4110.
40. Gaiani, S., Ferrari, E., Gozzi, M., Di Giovanni, M.T., Lassinantti Gualtieri, M., Colombini, E., Veronesi, P., 2023, *Impact of Post-Process Heat Treatments Performed on Ti6Al4V Titanium Alloy Specimens Obtained Using LPBF Technology*, Technologies, 11(4), 100.
41. Haque, R., Sekh, M., Kibria, G., Haidar, S., 2023, *Improvement of surface quality of Ti-6Al-4V alloy by powder mixed electrical discharge machining using copper powder*, Facta Universitatis Series Mechanical Engineering, 21(1), pp. 63-79.
42. ISO 4288:1996, *Geometrical Product Specifications (GPS) - Surface texture: Profile method - Rules and procedures for the assessment of surface texture*.
43. ISO 3274:1996, *Geometrical Product Specifications (GPS) - Surface texture: Profile method - Nominal characteristics of contact (stylus) instruments*.
44. Townsend, A., Senin, N., Blunt, L., Leach, R.K., Taylor, J.S., 2016, *Surface texture metrology for metal additive manufacturing: a review*, Precision Engineering, 46, pp. 34-47.
45. Spierings, A.B., Herres, N., Levy, G., 2011, *Influence of the particle size distribution on surface quality and mechanical properties in AM steel parts*, Rapid Prototyping Journal, 17(3), pp. 195-202.
46. Wilson-Heid, A.E., Wang, Z., McCornac, B., Beese, A.M., 2017, *Quantitative relationship between anisotropic strain to failure and grain morphology in additively manufactured Ti-6Al-4V*, Materials Science and Engineering A, 706, pp. 287-294.
47. Cao, F., Zhang, T., Ryder, M.A., Lados, D.A., 2018, *A Review of the Fatigue Properties of Additively Manufactured Ti-6Al-4V*, Jom, 70(3), pp. 349-357.
48. Viale, V., Stavridis, J., Salmi, A., Bondioli, F., Saboori, A., 2022, *Optimisation of downskin parameters to produce metallic parts via laser powder bed fusion process: an overview*, International Journal of Advanced Manufacturing Technology, 123, pp. 2159-2182.
49. Gockel, J., Sheridan, L., Koerper, B., Whip, B., 2019, *The influence of additive manufacturing processing parameters on surface roughness and fatigue life*, International Journal of Fatigue, 124, pp. 380-388.
50. Elsayed, M., Ghazy, M., Youssef, Y., Essa, K., 2019, *Optimization of SLM process parameters for Ti6Al4V medical implants*, Rapid Prototyping Journal, 25(3), pp. 433-447.
51. Kruth, J.P., Froyen, L., Van Vaerenbergh, J., Mercelis, P., Rombouts, M., Lauwers, B., 2004, *Selective laser melting of iron-based powder*, Journal of Materials Processing Technology, 149(1-3), pp. 616-622.
52. Mumtaz, K., Hopkinson, N., 2009, *Top surface and side roughness of Inconel 625 parts processed using selective laser melting*, Rapid Prototyping Journal, 15(2), pp. 96-103.
53. Hassanin, H., El-Sayed, M.A., Ahmadein, M., Alsaleh, N.A., Ataya, S., Ahmed, M.M.Z., Essa, K., 2023, *Optimising Surface Roughness and Density in Titanium Fabrication via Laser Powder Bed Fusion*, Micromachines, 14(8), 1642.